Accepted Manuscript

A novel type heterojunction photodiodes formed junctions of Au/LiZnSnO and LiZnSnO /p-Si in series

H. Aydin, A. Tataroğlu, Ahmed A. Al-Ghamdi, F. Yakuphanoglu, Farid El-Tantawy, W.A. Farooq

PII:	S0925-8388(14)02678-4
DOI:	http://dx.doi.org/10.1016/j.jallcom.2014.11.035
Reference:	JALCOM 32584
To appear in:	*Journal of Alloys and Compounds*
Received Date:	23 September 2014
Revised Date:	1 November 2014
Accepted Date:	4 November 2014

Please cite this article as: H. Aydin, A. Tataroğlu, A.A. Al-Ghamdi, F. Yakuphanoglu, F. El-Tantawy, W.A. Farooq, A novel type heterojunction photodiodes formed junctions of Au/LiZnSnO and LiZnSnO /p-Si in series, *Journal of Alloys and Compounds* (2014), doi: http://dx.doi.org/10.1016/j.jallcom.2014.11.035

A novel type heterojunction photodiodes formed junctions of Au/LiZnSnO and LiZnSnO /p-Si in series

H. Aydin[a], A. Tataroğlu[b], Ahmed A. Al-Ghamdi[c] , F. Yakuphanoglu[a,c], Farid El-Tantawy[d], W.A. Farooq[e]

[a]Department of Metallurgical and Materials Science, Faculty of Engineering, Tunceli University, Tunceli, Turkey
[b] Department of Physics, Faculty of Science, Gazi University, Ankara, Turkey
[c]Department of Physics, Faculty of Science, King Abdulaziz University, Jeddah, Saudi Arabia
[d]Department of Physics, Faculty of Science, Suez Canal University, Ismailia, Egypt
[e]Physics and Astronomy Department, College of Science, King Saud University, Riyadh, Saudi Arabia

Abstract

Lithium-zinc-tin-oxide thin films were prepared by sol gel method. The structural and optical properties of the films were investigated. The optical band gaps of the LiZnSnO films were found to be 3.78 eV for 0 %at. Li, 3.77 eV for 1 %at. Li, 3.87 eV for 3 %at. Li and 3.85 eV for 5 %at. Li, respectively. Au/LiZnSnO/p-Si/Al photodiodes were fabricated using a lithium-zinc-tin-oxide (LZTO, Li-Zn-Sn-O) layer grown on p-Si semiconductor. The electrical characteristics of the photodiodes were analyzed by current-voltage, capacitance-voltage and conductance-voltage measurements. The reverse current of the diodes increases with both the increasing illumination intensity and Li content. It was found that the Li-doped ZTO photodiodes exhibited a better device performance than those with an undoped ZTO.

Keywords: *Photodiode; Lithium-zinc-tin-oxide (LZTO); Sol gel*

Corresponding author: fyhanoglu@firat.edu.tr (F.Yakuphanoglu)
Tel:+90 4242370000-3496
Fax:+90 424 2330062

1. Introduction

Zinc-tin-oxide (ZTO, Zn-Sn-O) thin film attracts much attention due to its wide band gap, high visible transmittance, good n-type electrical conductivity, as well as its cheapness [1, 2]. Moreover, attractive attributes of ZTO include its tendency to possess an exceedingly smooth surface in thin films [3]. Thus, ZTO films can become the promising amorphous oxide semiconductors for oxide thin-film transistor applications. The ZTO films can be doped with various elements such as Zr, Ga, Al, Mg, La, and Ti to obtain the electrical performance devices [4-9].

A photodiode is a semiconductor device that transforms light into current and is designed to operate in reverse bias. Also, the photodiode has a depleted semiconductor region with a high electric field that serves to separate photo-generated electron-hole pairs. When the photodiode exposed illumination intensity, the electron-hole pairs occur near the junction interface and then they separated under electric field but this separated is more effective at in the reverse bias region due to the high value of electric field. Electron-hole pairs, which are absorbed in the quasi-neutral regions, can still contribute to the photocurrent generated within one diffusion length of the depletion region. Furthermore, carriers photo-generated in the depletion region are swept by the built-in field and flow as a drift current. Therefore, the photo-response effect in the reverse bias region is considerable higher than the forward bias region and the variation of photocurrent with light intensity was investigated in the reverse bias [10-13].

In present paper, we have fabricated LiZnSnO/p-Si photodiodes for the first time. The effects of Li addition on electrical characteristics of the photodiodes have been investigated using current-voltage, capacitance-voltage and conductance-voltage measurements.

2. Experimental details

The used precursors are lithium nitrate, tin chloride and zinc acetate. ZnSnO films were doped with various molar ratios of lithium: Li:(Zn+Sn) = 1:3:5. Firstly, the lithium nitrate, tin chloride and zinc acetate precursors were dissolved in 2-methoxyethanol under stirring for 30 min and then, ethanolamine was added to this solution and then, was stirred for 30 min at 60 ^{o}C on a hot plate. The LiZnSnO gel solutions were obtained. To prepare the diodes, firstly, p-Si substrates were used and an ohmic contact was prepared on back side of p-Si substrates by evaporating of Al metal. The prepared Al/p-Si contact was annealed at 570 ^{o}C for 5 min in nitrogen atmosphere. The prepared gel solutions of LiZnSnO samples were coated on p-type silicon wafer having ohmic Al contact using a spin coater with 4000 rpm for 30 s and dried at 150 ^{o}C for 10 min. The coating procedure was repeated for 10 times. Then, the obtained solid films were annealed at 400 ^{o}C for 1h. The top contact was prepared by evaporating of gold metal using a sputtering system to obtain a novel type heterojunction diode formed junctions of Au/LiZnSnO and LiZnSnO /p-Si in series. The film thicknesses of the 0at.% LiZnSnO , 1at.% LiZnSnO, 3at.% LiZnSnO and 5at.% LiZnSnO were determined using a PARK system XE100 atomic force microscopy and were found to be 356±5, 221±2, 295±3 and 300±4 nm, respectively.

The I-V, C-V and G-V measurements of the prepared diodes were carried out using a Keithley 4200 semiconductor characterization system. The photoresponse characteristics of the diodes were measured under a solar simulator and the intensity of the light was measured by solar power meter (Model TM-206). The reflectance spectra of the films were performed directly using a Shimadzu 3600 UV-VIS-NIR spectrometer attached an integrating sphere. X-ray diffraction patterns (XRD) of the LiZnSnO films were performed by BRUKER D8 diffractometer at room temperature.

3. Results and Discussion

3.1. Structural and optical properties of LiZnSnO films

Fig.1 shows AFM images of the LiZnSnO films. As seen in Fig.1, the surface morphology of the films is changed with Li dopant. The surface roughness values of 0at.% LiZnSnO, 1at.% LiZnSnO, 3at.% LiZnSnO and 5at.% LiZnSnO films were determined to be 7.32 nm, 15.77 nm, 16.86 nm and 8.11 nm, respectively. The grain sizes of the 0at.% LiZnSnO, 1at. LiZnSnO, 3at.% LiZnSnO and 5at.% LiZnSnO films were found to be 50-65 nm, 170-184 nm, 110-121 nm and 80-132 nm, respectively. The grain size is increased with Li dopant with respect to the grain size of ZnSnO film.

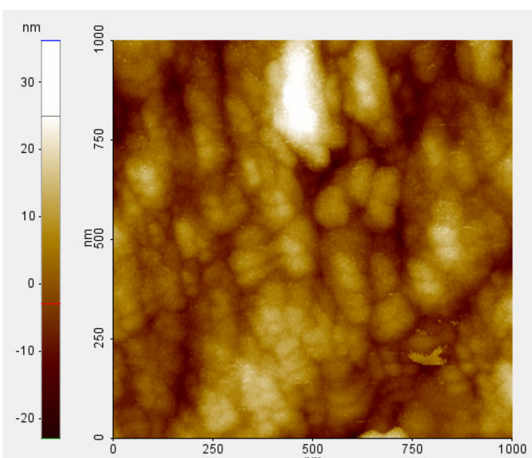

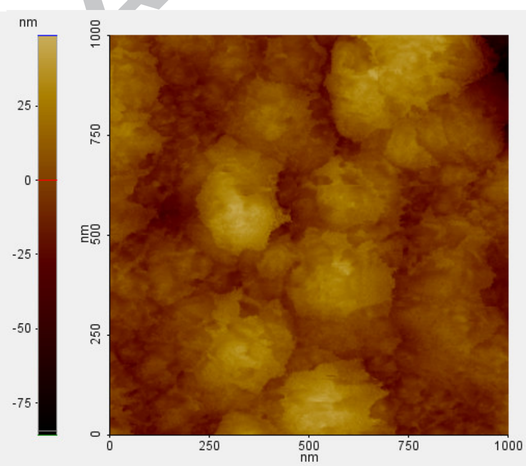

-a- **-b-**

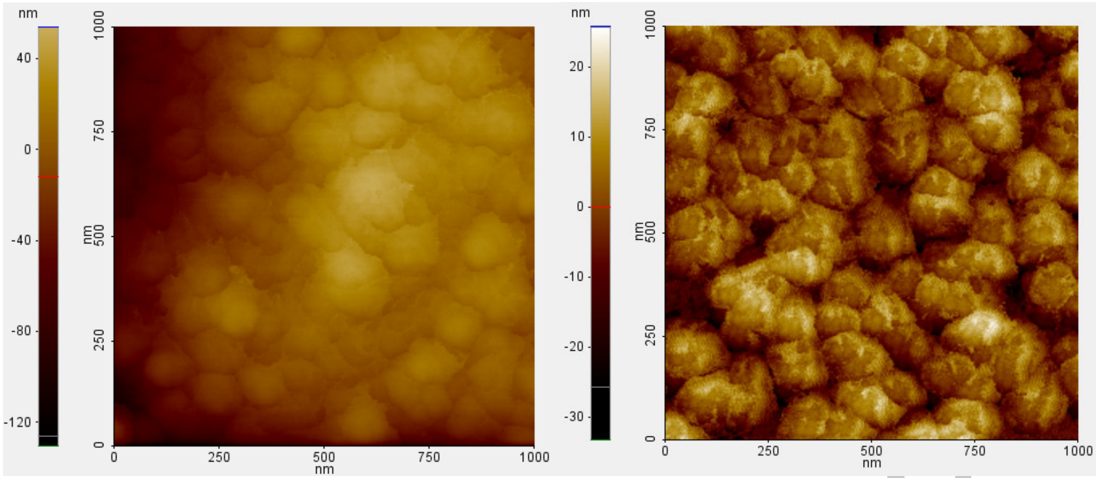

-c- **-d-**

Fig.1. AFM images of the LiZnSnO films a) 0at.% LiZnSnO b) 1at.% LiZnSnO c) 3at.% LiZnSnO d) 5at.% LiZnSnO

X-ray diffraction patterns (XRD) of the LiZnSnO films are shown in Fig.2. As seen in Fig.2, XRD patterns indicate some peaks. The first broad peak observed from 15 to 30^{o} and second peak observed from 30 to 40^{o} are resulted from the glass substrate. Another prominent peak was not observed in XRD patterns of LiZnSnO films. This suggests that the LiZnSnO films have an amorphous phase.

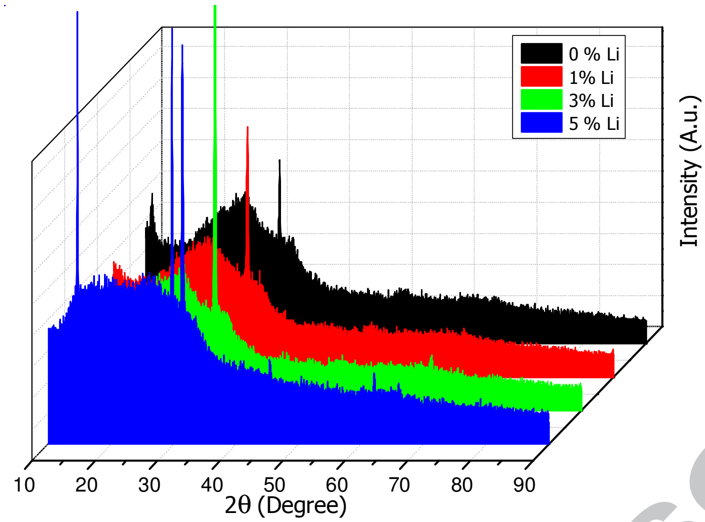

Fig.2 X-ray diffraction patterns of the LiZnSnO films

The transmittance spectra of the LiZnSnO films are shown in Fig. 3. It is seen that the films are transparent and their transparency is changed from 20 % to 75% between 300 and 1200 nm. The optical band gap of the films can be determined by the well-known relation

$$\alpha h\nu = B(h\nu - E_g)^n \quad (1)$$

where α is the optical absorption coefficient, B is a constant coefficient, hν is the photon energy and E_g is the optical band gap. In order to determine the optical band gap of the films, the plots of $(\alpha h\nu)^2$ versus hν are shown in Fig.4.

The optical band gaps of the LiZnSnO films were found to be 3.78 eV for 0at.% Li, 3.77 eV for 1at.% Li, 3.87 eV for 3at.% Li and 3.85 eV for 5at.% Li. The optical band gap of the films is changed with Li content. The optical band gap of the studied zinc tin oxide was found to be 3.78 eV. It is well known that the optical band gap of zinc tin oxide thin films is the range of 3.3–3.9 eV with a direct optical band gap [3]. The optical band gap of zinc tin oxide (ZTO) thin films deposited by thermal atomic layer deposition is increased from 3.4 to 4.6 eV with tin content and then, it is decreased [14]. These results indicate that the increase in optical band gap of the films is results from the chemical composition or structural variations of the zinc tin oxide thin films with Li content.

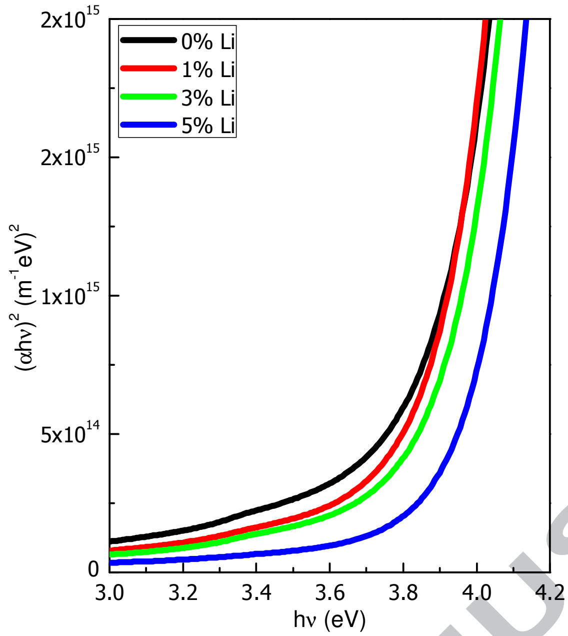

Fig.4a Plots of $(\alpha h\nu)^2$ vs. hν of LiZnSnO films

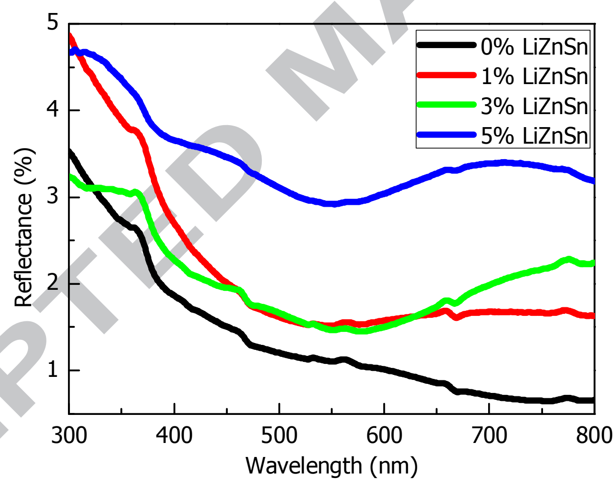

Fig.4b Plots of R vs. wavelength of the LiZnSnO films

The reflectance of the films is changed with Li content. After 500 nm, the reflectance is increased with decreasing wavelength and also with Li content. The increase in reflectance of the films is due to decrease in absorption of the films and this change confirms that Li atoms incorporated in Zn-Sn-O lattice. For optical applications of these films, the optical constant such as refractive index should be determined. For this, the complex refractive index of the films is as follows:

$$n^{*}(\lambda) = n(\lambda) + ik(\lambda) \tag{2}$$

where n is the refractive index and k is the extinction coefficient. The refractive index of the films can be determined by the following relation [15].

$$n = \left(\frac{1+R}{1-R}\right) + \sqrt{\frac{4R}{(1-R)^2} - k^2} \tag{3}$$

Where R is the reflectance and k is the extinction coefficient. The refractive index of the films are determined using Eq.3 and is shown in Fig.5. As seen in Fig.5, the refractive index is increased with Li content.

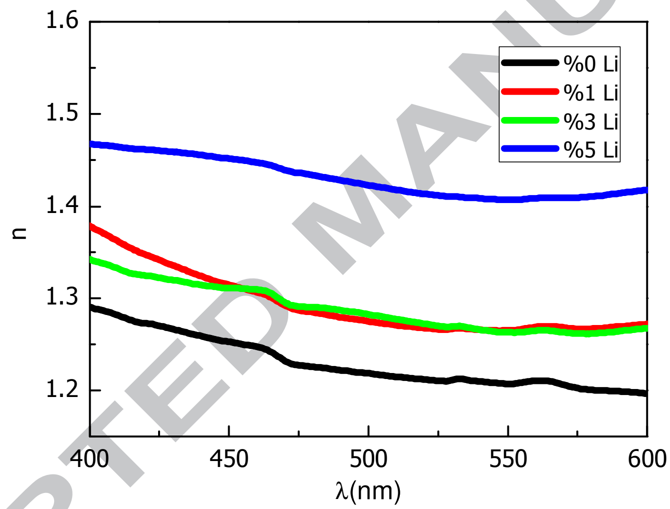

Fig.5 Plots of refractive index of the LiZnSnO films

3.2. Current-voltage characteristics of the diodes

Figs. 6(a), (b) and (c) show semi-logarithmic I-V characteristics of the photodiodes under dark and various illuminations. As seen in Fig. 6(a-c), the diodes exhibited a rectifying behavior. This behavior of the diodes can be analyzed using thermionic emission (TE) theory. In this theory, the electrons transports over a potential barrier. Thermionic emission current assumes that only electrons with energies greater than the energy of the potential barrier add to the current flow. According to this theory, the current (I) is described by the following equation [16-17]

$$I = A A^{*} T^{2} \exp\left(-\frac{q\Phi_{B0}}{kT}\right)\exp\left(\frac{qV}{nkT}\right) \tag{4}$$

where I_0 is the saturation current and n is the ideality factor, A is the diode contact area ($3.14x10^{-2}$ cm^2), A* is the Richardson constant of 32 $Acm^{-2}K^{-2}$ for p-type silicon and Φ_{B0} is the zero-bias barrier height. A change in the ideality factor over the life of the diode is an indicative of the variation in metal-semiconductor interface. This parameter is a measure of the conformity of a diode current to be pure TE.

As seen in Fig. 6(a), (b) and (c), the reverse current at a given voltage of the photodiode with different Li content under illumination is higher than that of the current under dark. In other words, the reverse current of the photodiodes increases with the increasing illumination intensity. This indicates that the prepared diodes exhibit a photodiode behavior. When the semiconductor device is illuminated, electrons in the valence band of the semiconductor absorb energy, and they are able to jump to the conduction band. Also, the ln(I)-V curves of the photodiodes deviate from linearity at higher forward-bias voltages due to the effects of some factors such as series resistance, interface states, etc [15,18-20]. The values of barrier height (Φ_{B0}) were calculated from the intercept of the forward bias In(I)-V plots of the photodiodes and were found to be about 0.69 for 0at.% Li, 0.67 for 1at.% Li, and 0.65 eV for 3at.% Li, respectively. It is seen that the barrier height is decreased with increasing Li content.

The value of ideality factor (n) were calculated using Eq. (4) from the slope of the forward bias In(I)-V plots of the photodiodes with different Li content for all conditions and were found to be about 4.50 for 0at.% Li, 4.55 for 1at.% Li and 4.60 for 3at.% Li, respectively. The obtained n value of the diodes is higher than unity. The high value of n is attributed to the presence of inhomogenities of the barrier height, the particular distribution of the interface states, series resistance, the image force effect, generation-recombination currents within the space-charge region, wide distribution of low Schottky barrier height patches at metal/semiconductor interface, and tunneling [20-30].

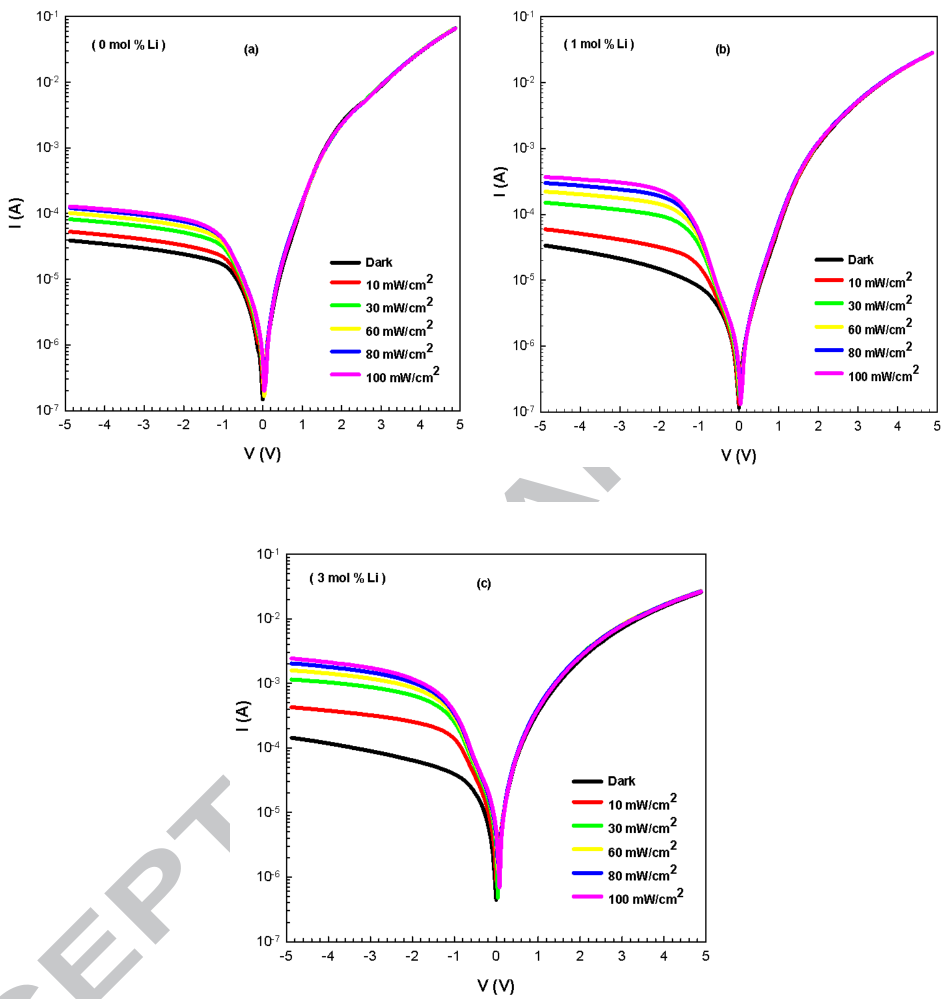

Fig. 6. Semi-logarithmic I-V characteristics of the photodiodes with different the addition of Li to the ZTO under dark and various illuminations: a) 0at.% LiZnSnO b) 1at.% LiZnSnO c) 3at.% LiZnSnO

Fig. 7 shows semi-logarithmic I-V characteristics of the photodiodes at 100 mW/cm^2 illumination intensity. As seen in Fig. 6, the value of reverse current increases with the increasing Li content. This might be attributed to the increase of carrier concentration caused by the addition of Li.

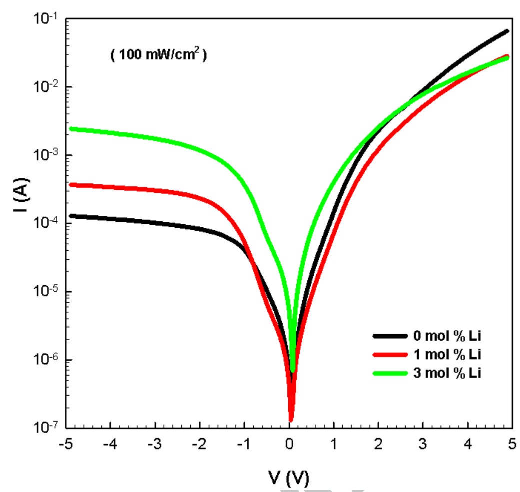

Fig. 7. Semi-logarithmic I-V characteristics of the photodiodes at 100 mW/cm^2 illumination intensity.

The variation in the photocurrent with illumination intensity can be analyzed by the following relation [31-33],

$$I_{PH} = AP^{m} \tag{5}$$

where I_{PH} is the photocurrent, A is a constant, m is an exponent and P is the illumination intensity. The obtained m value suggests that the photoconduction mechanism of the diodes exhibited a linear behavior. Also, the obtained m value in the range of 0.5 to 1 implies the presence of continuous distribution of trap levels. As seen in Fig. 6, the reverse current under a certain illumination is higher than the current under dark. This confirms the photodiode behavior. To analyze the photoconducting mechanism of the photodiodes, the photocurrent plots are plotted as a function of Li content and are given in Fig. 8. The values of m for 0, 1 and 3% Li contents were found to be about 0.39, 0.78 and 0.75, respectively.

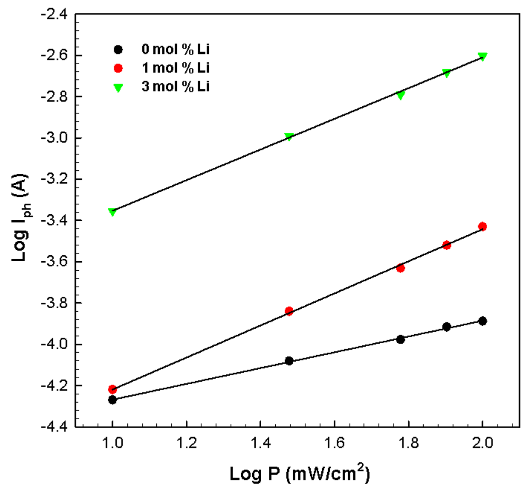

Fig. 8. Plots of log(I_{PH}) vs log(P) of the photodiodes with different Li contents (at -5 V)

In addition, the transient photocurrent study is a well-known technique using to understand the transport mechanism of any photodiode. The transient photocurrent measurement of the photodiodes with different Li content was performed under illumination intensity of 100 mW/cm^2 and is given in Fig. 9. As seen in Fig. 9, after turning on the illumination, the photocurrent of the diode rapidly increases to a certain level and then gradually tends to the maximum value. When the photodiode was illuminated, the number of photogenerated charge carries increase with the illumination and the electrons contribute to the current. On the other hand, after turning on the illumination, the photocurrent of the diode decreases due to the trapping of the charge carriers in the deep levels and comes back to its initial state. As a result, the fabricated photodiodes exhibits a good photoconducting behavior [34-38].

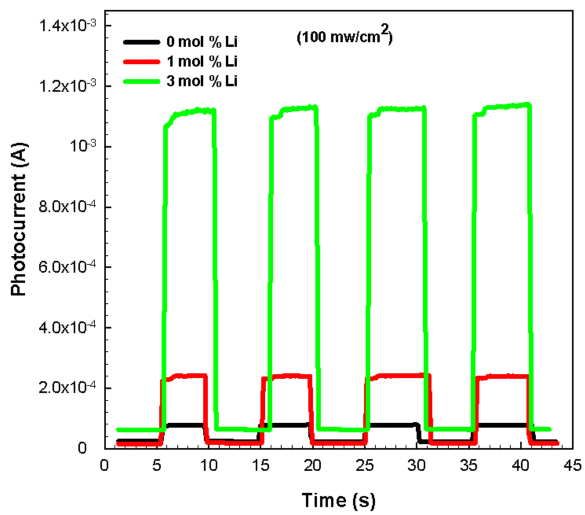

Fig. 9. Plots of photocurrent-time of the photodiodes with different Li content under 100 mW/cm^2 illumination intensity.

3.3. Capacitance-voltage and conductance-voltage characteristics

The capacitance-voltage plots of the photodiodes with various Li contents are given in Fig. 10. As seen in Fig. 10 (a), (b) and (c), the value of C remains almost constant with the decreasing reverse bias voltage. In forward bias voltage region, the value of C is decreased with the increasing frequency. The higher values of C at lower frequencies can be attributed to the presence of continuous distribution of the interface states. In other words, at lower frequencies, the interface charges can follow the ac signal and they contribute to the capacitance [39-45].

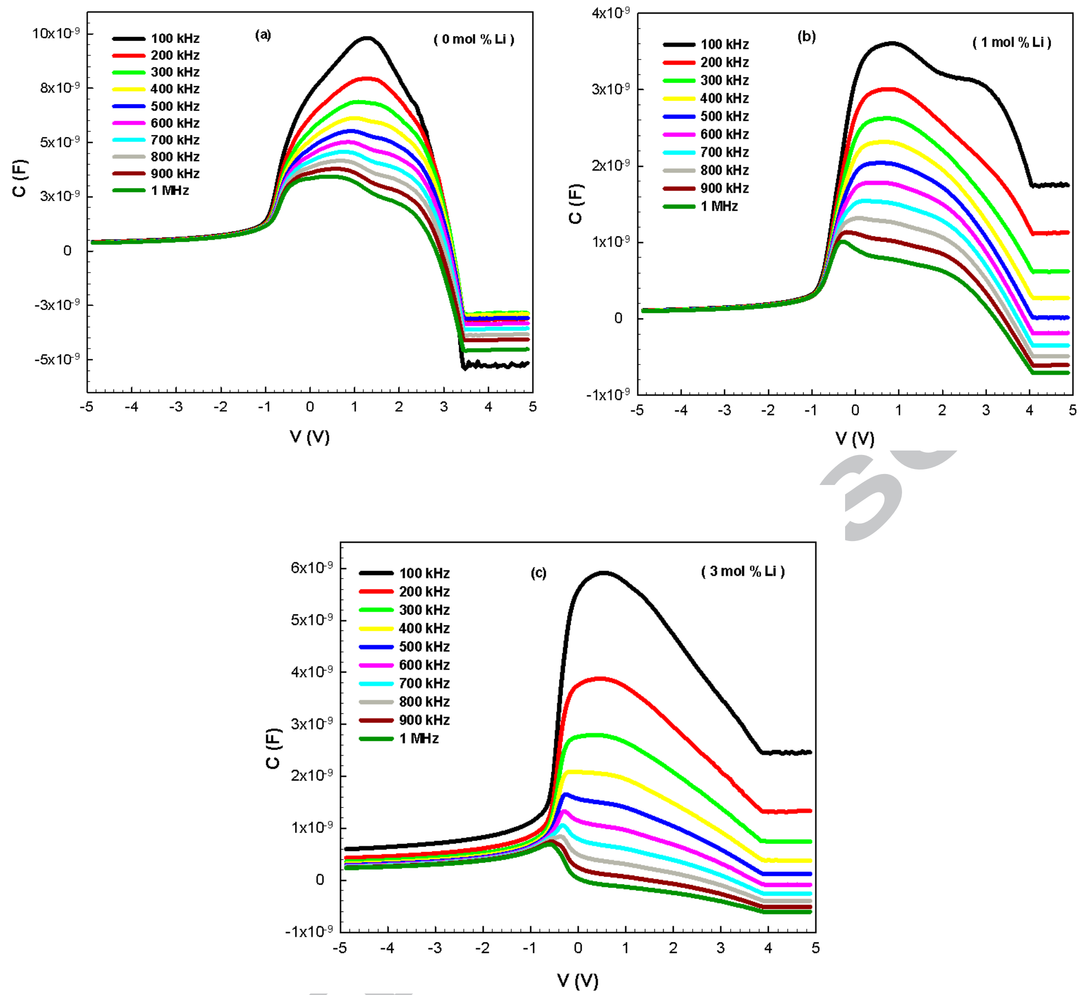

Fig. 10. The capacitance-voltage (C-V) plots of the photodiodes with various Li contents a) 0at.% LiZnSnO b) 1at.% LiZnSnO c) 3at.% LiZnSnO

In addition, the forward bias C-V curves of the photodiodes with different Li content show an abnormal behavior. After the crossing point, the C values increase with increasing frequency. The negative capacitance (NC) behavior of the C-V curves at each frequency may be explained by considering the loss of interface charges at occupied states below Fermi level. The NC has been detected in many electronic and optoelectronic devices, such as polymer light emitting diodes, metal-semiconductor interface, metallic nanoparticles embedded in dielectric, p-n junction, quantum well infrared photodetectors, etc. [46-51].

The microscopic physical mechanisms of the negative capacitance in various devices are obviously different and have been ascribed mainly to the contact injection, interface states, or minority-carrier injection effects.

The conductance-voltage (G-V) plots of the photodiodes with various Li contents are shown in Fig. 11. As seen in Fig. 11(a), (b) and (c), the value of G increases with the increasing frequency in the forward bias voltage region. This confirms the presence of the interface states. The value of G remains almost constant in the reverse bias voltage region.

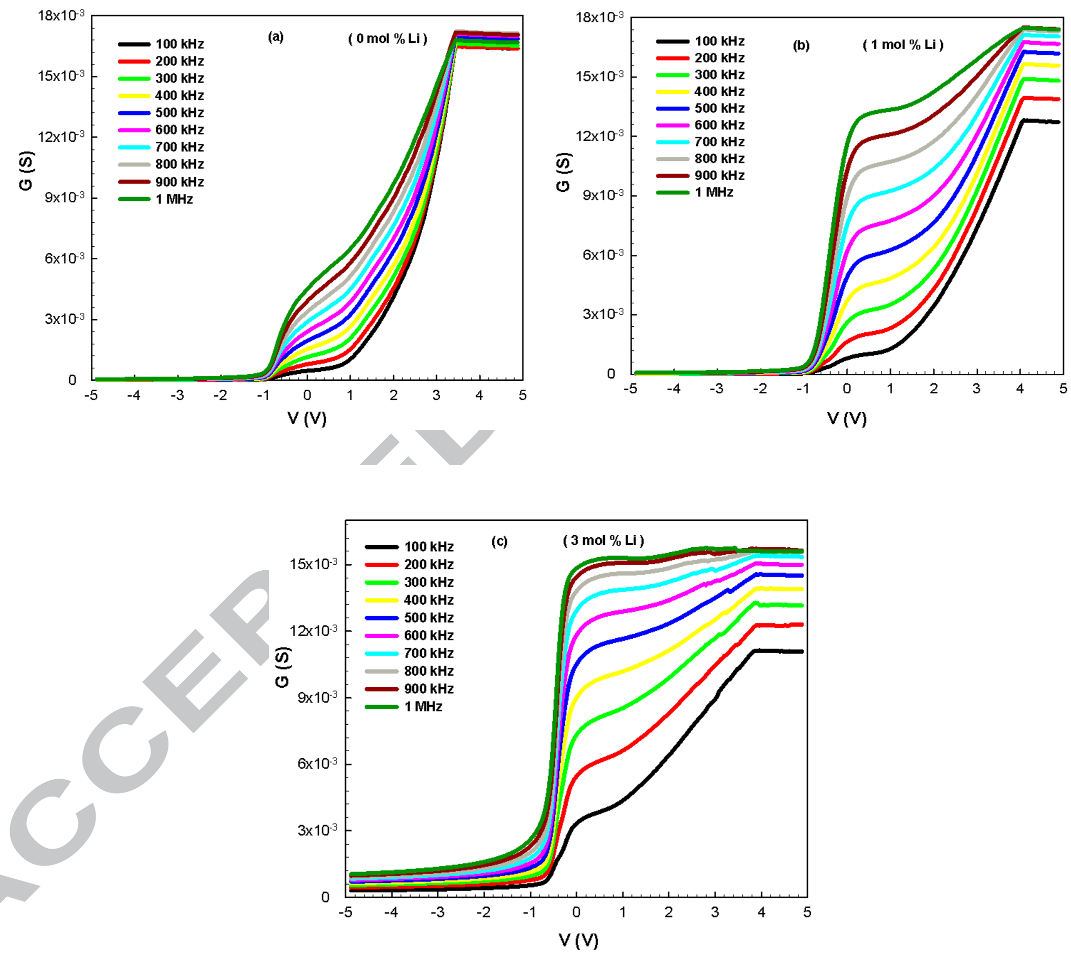

Fig. 11. The conductance-voltage (G-V) plots of the photodiodes

a) 0at.% LiZnSnO b) 1at.% LiZnSnO c) 3at.% LiZnSnO

The series resistance (R_s) is the most important parameter that causes the electrical parameters of semiconductor device. In order to determine the values of R_s , we can use the total impedance of the parallel RC circuit model. The measured impedance (Z_{ma}) at strong accumulation region of device is equivalent to the total circuit impedance as [17,19]:

$$Z_{ma} = \frac{1}{G_{ma} + j\omega C_{ma}} \tag{6}$$

Comparing the real and imaginary part of the impedance, the real value of R_s of the device can be subtracted from the measured capacitance (C_{ma}) and conductance (G_{ma}) in the strong accumulation region at sufficiently high frequency. The value of R_s is calculated by the following relation,

$$R_s = \frac{G_{ma}}{G_{ma}^2 + (\omega C_{ma})^2} \tag{7}$$

The series resistance values are determined and are given in Fig.12 (a), (b) and (c). It is seen that the series resistance decreases with the increasing frequency. This frequency dependence of R_s is the result of frequency-dependent charges such as interface charge, fixed oxide charge, oxide-trapped charge and mobile oxide charge [52-56]. Moreover, the R_s-V plots give a peak at about -1 V for 0 and 1at.% Li and the peak intensity is decreased with the increasing frequency. This indicates the presence of interface states in the interface of the photodiodes.

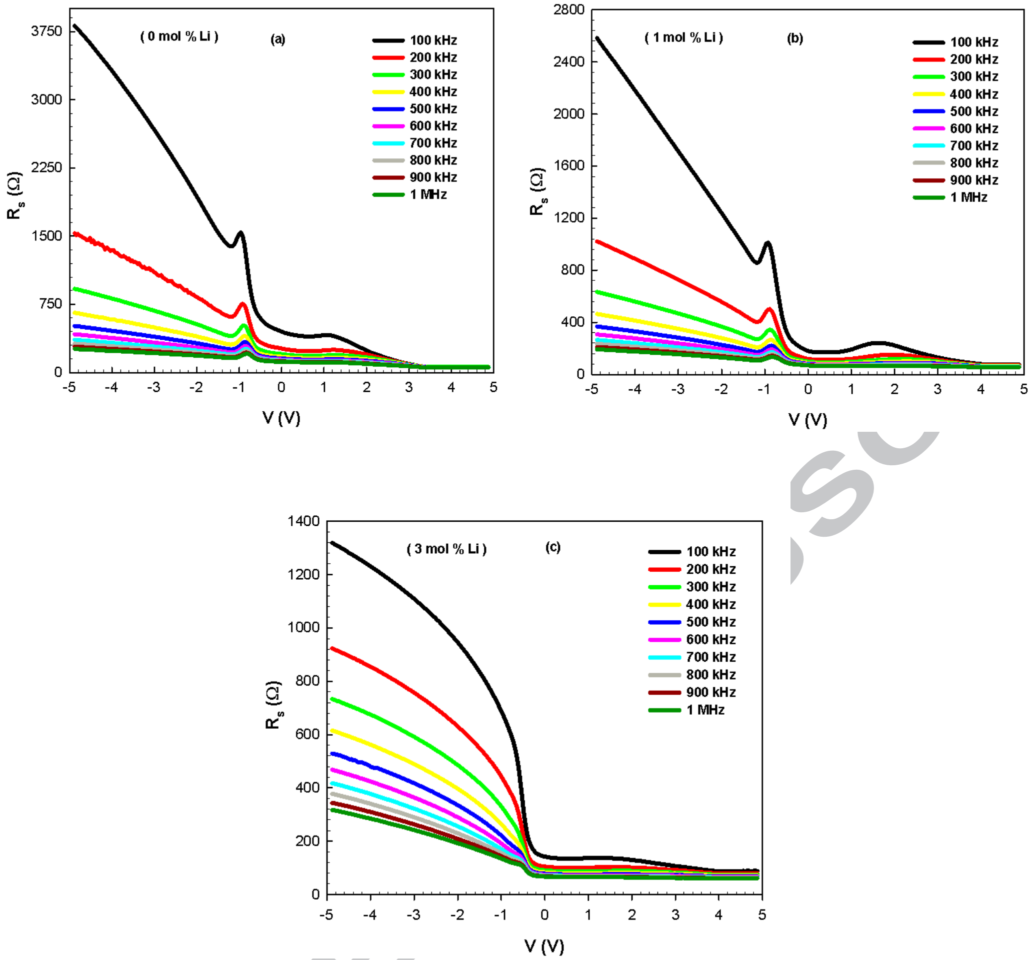

Fig. 12. The series resistance-voltage (R_s-V) plots of the photodiodes with various Li contents at various frequencies.

4. Conclusions

The effects of Li content on the electrical characteristics of the photodiodes with LZTO interfacial layer. The photocurrent of the diodes is increased with the increasing Li content. The I-V characteristics of the diodes under various illumination intensities suggest that the photoresponse of the studied photodiodes is very sensitive to illumination intensity. In addition, the C-V and G-V measurements indicate that the value of C and G/ω depends on applied voltage and frequency. The obtained results suggest that the photodiodes with Li-doped ZTO interfacial layer exhibited a better device performance than those with an undoped ZTO.

References

1. Masuda S, Kitamura K, Okumura Y, Miyatake S, Kawai T (2003), J. Appl. Phys. 93, 1624

2. Wang CH, Chen SW, Wu JM, Wei CN, Bor HY (2011) Electrochem. Solid-State Lett. 14:P5-P8.

3. Chiang HQ, Wager JF, Hoffman RL, Jeong J, Keszler DA (2005) Appl. Phys. Lett. 86:013503 (3 pages).

4. Rim YS, Kim DL, Jeong WH, Kim HJ (2010) Appl. Phys. Lett. 15:233502 (3 pages).

5. Jeong Y, Song K, Jun T, Jeong S, Moon J (2011) Thin Solid Films 519:6164-6168.

6. Cho D-H, Yang S, Byun C, Shin J, Ryu MK, Ko Park S-H, Hwang C-S, Chung SM, Cheong W-S, Yoon SM, Chu H-Y (2008) Appl. Phys. Lett. 93:142111 (4 pages).

7. Kim HB, Lee HS (2014) Thin Solid Films 550:504-508.

8. Yue L, Pu H, Pang S, Li H, Zhang Q (2012) Europhys. Lett. 97:67006 (5 pages).

9. Jung HY, Park SY, Kim J-I, Yang H, Choi R, Kim D-H, Bae J-U, Shin W-S, Jeong JK (2012) Thin Solid Films 522:435-440.

10. Edited by I. Yun, Photodiodes-from Fundamentals to Applications, InTech, Croatia, 2012.

11. Ng KK, Complete Guide to Semiconductor Devices, 2nd Ed., John Wiley& Sons, New York, 2002.

12. Edited by G.-F. Dalla Beta, Advances in Photodiodes, InTech, Croatia, (2011).

13. Schneider MV (1966) Bell Syst. Tech. J. 45:1611-1618.

14. Mullings MN., Hägglund C, Tanskanen JT, Yee Y, Geyer S, Bent SF (2014), Thin Solid Films 556:186–194

15. Yakuphanoglu F (2006) Optical Materials 29:253–256

16. Rhoderick EH, Williams RH, Metal-Semiconductor Contacts, 2nd Ed., Clarendon Press, Oxford, 1988.

17. Nicollian EH, Goetzberger A (1967) Bell Syst. Tech. J. 46:1055-1133.

18. Sze SM, Crowell CR, Kahng D (1964) J. Appl. Phys. 35:2534-2536.

19. Nicollian EH, Goetzberger A (1965) Appl. Phys. Lett. 7:216-219.

20. Tung RT (2001) Phys. Rev. B 64:205310 (15 pages).

21. Yahia IS, Yakuphanoglu F, Chusnutdinow S, Wojtowicz T, Karczewski G (2013) Curr. Appl. Phys. 13:537-543.

22. Tataroğlu A, Hendi AA, Alorainy RH, Yakuphanoğlu F (2014) Chin. Phys. B 23: 057504 (5 pages).

23. Karataş Ş, Altındal Ş, Türüt A, Özmen A (2003) Appl. Surf. Sci. 217:250-260.

24. Sharma M, Tripathi SK (2013) Appl. Phys. A 113:491-499.

25. Alahmed ZA, Mansour ShA, Enver Aydın M, Yakuphanoglu F (2013) Solid State Commun. 163:23-27.

26. Birel O, Kavasoglu N, Kavasoglu AS, Dincalp H, Metin B (2013) Physica B 412:64-69.

27. Kaushal P, Chand S, Osvald J (2013) Inter. J. Electron.100:686-698.

28. Tataroğlu A (2013) Chin. Phys. B 22:068402 (6 pages).

29. Farag AAM, Osiris WG, Ammar AH, Mansour AM (2013) Synthetic Met. 175:81-87.

30. Sakr GB (2013) Mater. Chem. Phys. 138:951-955.

31. Kazım S, Ali V, Zulfequar M, Mazharul Haq M, Husain M (2007) Physica B 393:310-315.

32. Gupta RK, Cavas M, Al-Ghamdi AA, Gafer ZH, El-Tantawy F, Yakuphanoğlu F (2013) Solar Energy 92:1-6.

33. Lee JM, Shin JC, Hwang CS, Kim HJ (1998) J. Vac. Sci. Technol. A 16:2768-2771.

34. Bube RH, Photoconductivity of Solids, Wiley, New York, 1960.

35. Kazım S, Ali V, Zulfequar M, Mazharul Haq M, Husain M (2007) Physica B 393:310-315

36. Phan D-T, Gupta RK, Chung G-S, Al-Ghamdi AA, Al-Hartomy OA, El- Tantawy F, Yakuphanoğlu F (2012) Solar Energy 86 2961-2966.

37. Cheng G, Wu X, Liu B, Li B, Zhang X, Z. Du (2011) Appl. Phys. Lett. 99:203105 (pages).

38. Yakuphanoğlu F, Farooq WA (2011) Mater. Sci. Semicond. Process. 14:207-211.

39. Nicollian EH, Brews JR, MOS Physics and Technology, Wiley, New York, 1982.

40. J.H. Werner, Metallization and Metal-Semiconductor Interface, Plenum, New York, 1989, pp. 235-256.

41. Tataroğlu A, Altındal Ş (2008) Microelectron. Eng. 85:2256-2260.

42. Gupta SK, Shankar B, Taube WR, Singh J, Akhtar J (2014) Physica B 434:44-50.

43. Pratap Reddy MS, Lee J-H, Jang J-S (2013) Synthetic Met. 185-186:167-171.

44. Kim H, Kim H, Kim D-W (2014) Vacuum 101:92-97.

45. Fouad SS, Sakr GB, Yahia IS, Abdel-Basset DM, Yakuphanoğlu F (2014) Mater. Res. Bull. 49:369-383.

46. Arslan E, Şafak Y, Altındal Ş, Kelekci Ö, Özbay E (2010) J. Non-Crys. Solids 356:1006-1011.

47. Werner J, Levi AFJ, Tung RT, Anzlowar M, Pinto M (1988) Phys. Rev. Lett. 60:53-56.

48. Korucu D, Türüt A, Altındal Ş (2013) Curr. Appl. Phys. 13:1101-1108.

49. Shulman J, Tsul S, Chen F, Xue YY, Chu CW (2007) Appl. Phys. Lett. 90:032902 (3 pages).

50. Rahman A, Sanyal MK (2009) Appl. Phys. Lett. 94:242102 (3 pages).

51. Wu X, Yang ES, Evans HL (1990) J. Appl. Phys. 68:2845-2848.

52. Chatterjee S, Kuo Y, Lu J (2008) Microelectron. Eng. 85:202-209.

53. Karataş Ş, Yakuphanoğlu F, Amanullah FM (2012) J. Phys. Chem. Solids 73:46-51.

54. Altındal Ş, Uslu H (2011) J. Appl. Phys. 109:074503 (7 pages).

55. Cherif A, Jomni S, Mliki N, Beji L (2013) Physica B 429:79-84.

56. Cova P, Singh A (1990) Solid-State Electron. 33:11-19.

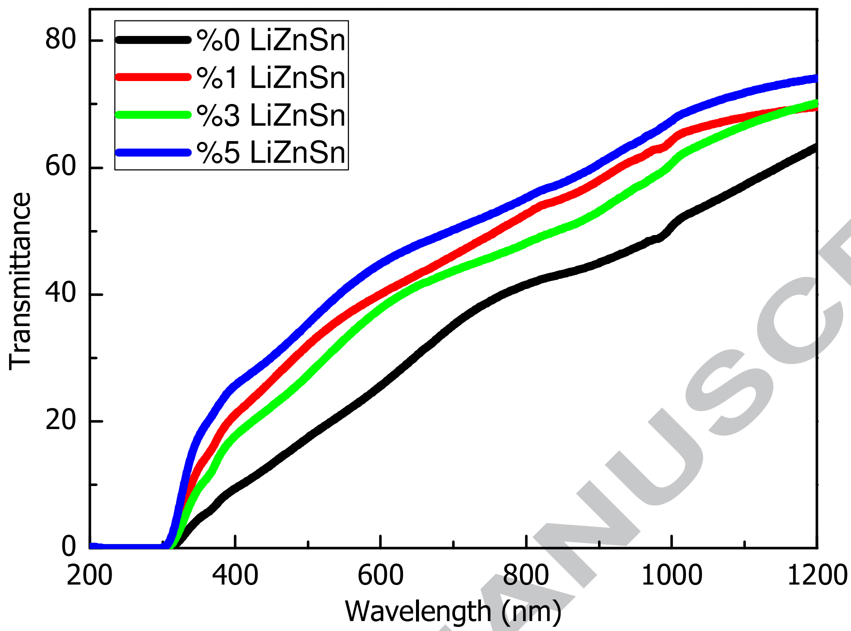

Fig.3. Transmittance spectra of the LiZnSnO films

Highlights

1. Lithium-zinc-tin-oxide thin films were prepared by sol gel method.
2. The Au/LiZnSnO/p-Si/Al photodiodes were fabricated using a lithium-zinc-tin-oxide (LZTO, Li-Zn-Sn-O) layer grown on p-Si semiconductor.
3. The photodiodes with Li-doped ZTO interfacial layer exhibited a better device performance than those with an undoped ZTO.